Received: 29 September 2023 | Revised: 2 November 2023 | Accepted: 6 November 2023

DOI: 10.1002/cm.21809

RESEARCH ARTICLE

CYTOSKELETON WILEY

Mapping the cytoskeletal architecture of renal tubules and surrounding peritubular capillaries in the kidney

Girishkumar Kaitholil Kumaran[1] | Israel Hanukoglu[1,2]

[1]Laboratory of Cell Biology, Ariel University, Ariel, Israel

[2]Etgar College of Engineering and Technology, Tel Aviv, Israel

Correspondence
Israel Hanukoglu, Etgar College of Engineering and Technology, David Hackmey St. 15, Tel Aviv, Israel.
Email: mbiochem@gmail.com

Present address
Girishkumar Kaitholil Kumaran, CAMS Oxford Institute, Nuffield Department of Medicine, University of Oxford, Oxford, UK.

Funding information
Ariel University

Abstract

The human kidney includes ~1 million nephrons which are long U-shaped tubules with convoluted segments that serve as filtration units. During the passage of the ultrafiltrate through a nephron, electrolytes and nutrients are re-absorbed into peritubular capillaries. The fluid remaining in the distal end of the renal tubules flows through the collecting ducts into the ureter. In this study, we generated high-resolution images of mouse kidney sections using confocal microscopy with only two fluorescently tagged biomarkers, F-actin binding phalloidin and CD34 antibodies as a marker for blood vessels. In tile-scan images of entire sections of mouse kidney (composed of >1000 images), the tubule segments are easily identifiable by their F-actin bundles on cell borders and the outlines of the peritubular capillaries by CD34 immunofluorescence. In the inner stripe of the medulla, the vascular bundles composed of vasa recta (straight vessels) could be easily distinguished from the peritubular capillaries by their full circular shapes. The highly vascular inner medulla and the papilla similarly have straight capillaries. About 95% of kidney volume is composed of renal tubules and blood vessels. Thus, our results show that relatively simple cytoskeletal mapping can be used to visualize the structural organization of the kidney. This method can also be applied to examine pathological changes in the kidney.

KEYWORDS
actin, CD34, cell membrane, cytoskeleton, nephron

1 | INTRODUCTION

The kidney is responsible for many vital functions, including continuous filtration of the blood, excretion of metabolic waste products such as urea and creatinine, homeostasis of water and electrolyte levels, synthesis and secretion of various hormones including erythropoietin that stimulates red blood cell regulation, and renin that regulates blood pressure. About 20% of the cardiac output is channeled to the kidneys which represent less than 1% of the total body mass. The renal arteries branch out from the abdominal aorta and enter the hilum of the kidneys. In the kidney, the main artery branches, forming the segmental arteries. These branch further into interlobar arteries that supply blood to each kidney lobe via arcuate arteries (Al-Katib et al., 2017; Sequeira Lopez, 2016). The human kidney is composed of 4–18 similarly shaped lobes, also known as renal pyramids (Cullen-McEwen et al., 2016). Rodent kidneys have a single lobe, the structure and organization of which is highly similar to the lobes in human kidneys.

In all mammals, the process of blood filtration starts with the flow of blood into glomeruli, which are globular structures of intertwined capillaries. The glomeruli are located in the cortex of the kidney and receive their blood supply via afferent arterioles. As the blood flows through the glomerular capillaries, water, electrolytes, and small solutes, but not plasma proteins, pass through the capillary membrane into the Bowman's space surrounding the glomerulus. The filtered blood exits via the efferent arteriole and flows through a complex plexus of peritubular capillaries intertwined with the nephron tubules

(Sequeira Lopez, 2016). The blood in these capillaries drains into the cortical radiate veins connected to the arcuate vein.

The vascular trees formed by successive branchings of the renal artery have been visualized by renal micro-computer tomography (CT) images of rat kidneys (Nordsletten et al., 2006). These trees revealed that the arterial and the venous trees run in parallel. However, this CT imaging did not include the peritubular capillaries and the arterial and venous vasa recta. Fan et al. recently reported visualization of the intrarenal capillaries (including the peritubular and vasa recta capillaries) using a modified technique of filling the renal vasculature with a silicon rubber (Microfil) (Fan et al., 2019).

We undertook the present study to visualize the capillaries surrounding the kidney tubules and to generate a map of the capillaries in kidney sections. Recently, we described a simple method for identifying and visualizing renal tubules using actin cytoskeleton features (Kumaran & Hanukoglu, 2020). In the present study, we combined this method of visualizing renal tubules with the addition of a CD34 as a marker for endothelial cells and blood vessels. CD34 is a transmembrane glycoprotein encoded by the gene CD34, specifically expressed in hematopoietic progenitor cells and endothelial cells (Hassanpour et al., 2023; Rodrigues et al., 2023). A previous immunohistochemical study showed that anti-CD34 antibodies stain the glomerular capillaries in human kidneys (Pusztaszeri et al., 2006). Our results, for the first time, provide a global map of the endothelia in renal sections with high-resolution imaging of the peritubular capillaries surrounding the different nephron tubule segments identified by cytoskeletal mapping.

2 | METHODS

2.1 | Tissue preparation and cryosectioning

Mouse kidney tissues were obtained from adult male ICR mice (40–60 g) aged 6 to 12 weeks. The mice were housed in a standard cage at 25 °C with a 12 h dark/light cycle and ad-libitum access to food and water. The study protocol was approved by the Institutional Animal Ethics Committee of Ariel University (permit 32_12733_b019), according to the Ministry of Health guidelines.

The anesthetized animals were perfused before the kidneys were surgically removed. An intraperitoneal injection of 100 mg/kg ketamine and 5 mg/kg xylazine was used as the anesthetic. Phosphate-buffered saline, pH 7.4 (PBS), followed by 4% paraformaldehyde w/v (BDH Limited Poole, England) dissolved in PBS was used for cardiac perfusion. The extracted kidneys were cut into small blocks and left in 4% paraformaldehyde in PBS overnight at 4 °C. The kidney blocks were then put in 30% sucrose solution and left at 4 °C until they settled at the bottom of the tube.

For cryosectioning, the tissues were embedded and frozen at −20 °C using Tissue Tek OCT compound (Sakura, Netherlands). The frozen kidney blocks were sectioned using Slee MEV floor standing ECO cryostat (SLEE Medical GmbH, Germany). The chamber and objective temperatures were −25 °C and −20 °C, respectively. Sections were collected in wells of a 24-well plate in PBS containing 0.1% sodium azide.

2.2 | Fluorescent labeling

The kidney sections were treated with 4% paraformaldehyde w/v dissolved in PBS for 10 min. The sections were washed with PBS for 5 min twice and then permeabilized with 0.1% Tween-20 dissolved in PBS for 10 min. After permeabilization, the sections were blocked with 4% bovine serum albumin (BSA) w/v in PBS for 20 min.

To visualize the renal capillaries anti-CD34 (Abcam, #AB81289) antibodies were used. The tissue sections were incubated with anti-CD34 antibodies (1:100) in 4% BSA in PBS for 60 min. The tissue sections were then washed with PBS for 5 min, six times. After washing, the sections were incubated with Alexa Fluor 555 (Life Technologies, #A21428) secondary antibodies (1:200) in 4% BSA in PBS for 60 min. The tissue sections were washed again six times, 5 min each.

The actin filaments were stained by incubating CF488A-conjugated phalloidin (Biotium) (1:20) in 4% BSA in PBS for 60 min. The incubation was followed by washing with PBS three times for 5 min.

The nuclei were stained with DAPI (1:100) dissolved in 4% BSA in PBS for 2 min. The tissue sections were washed again in PBS twice, 5 min each.

After staining, the tissue sections were mounted on X-tra adhesive slides (Leica Biosystems, UK) using the anti-fade reagent n-propyl gallate (Sigma–Aldrich) 0.5% (w/v) in 100 mM phosphate buffered (pH 7.2) glycerol (90%).

2.3 | Confocal microscopy

The fluorescent-labeled tissue sections were imaged using an LSM 700 confocal microscope (Carl-Zeiss, Germany). To view the fluorescence of the biomarkers, we used excitation wavelengths of 555 nm, 488 nm, and 405 nm for AF555 secondary antibodies, CF488A, and DAPI, respectively. Tile-scan images were collected using 5% overlap and 40× oil-immersion objective. The images were stitched using ZEN 2012 Blue software using a correlation threshold of 0.40. FIJI/ImageJ was used to generate the final images from LSM files. 3D images in Figure 6d–f were generated by compiling images from z-stack optical sectioning of tissue sections as previously described (Sharma et al., 2020).

3 | RESULTS

In this study, we used high-resolution confocal microscopy to visualize the intricate spatial arrangement of peritubular capillaries and broader vascular network within different anatomical regions of mouse kidney

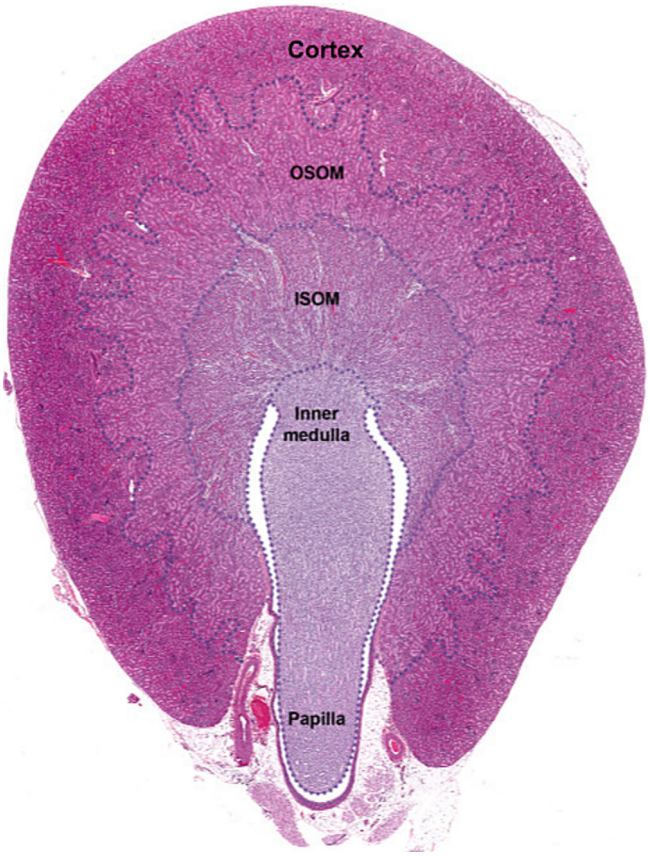

FIGURE 1 Cross section of a rat kidney delineating the main histological regions of the kidney: cortex, the outer medulla and its two sub-regions outer stripe (OSOM), and inner stripe (ISOM), the inner medulla, and papilla. *Source*: National Toxicology Program histopathology images.

using two biomarkers: (1) Phalloidin for the visualization of the actin cytoskeleton. (2) Anti-CD34 antibodies for mapping the peritubular capillaries and the blood vascular system. Kidneys have different layers within their structure due to the highly organized nature of nephrons. Commonly identified histological regions are the cortex, outer medulla (OSOM—outer stripe of outer medulla, ISOM—inner stripe of outer medulla), inner medulla, and papilla, as shown in Figure 1.

3.1 | Cortical region

Figure 2 presents a tile-scan image of a longitudinal section (~7.5 mm long) through the cortical region of the kidney composed of 1392 images. Both F-actin and CD34 fluorescence were strongest in the glomeruli (Figure 2). In the merged image, the glomeruli appear in yellowish-orange color, indicating that the phalloidin fluorescence (green) and CD34 immunofluorescence (red) are overlapping (Figure 2c). This overlap-dependent color shift is clearly visible in a magnified image of a glomerulus (Figure 3).

In a magnified view, the nephron tubule segments could be easily identified by the characteristic features we defined in our earlier study

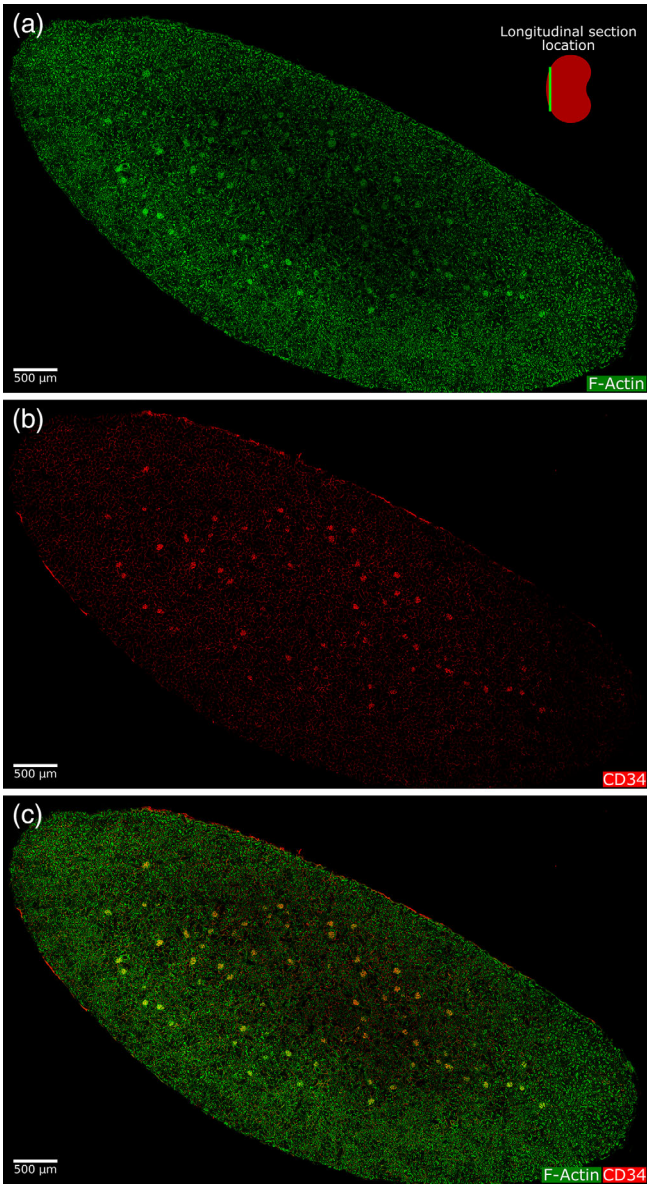

FIGURE 2 Actin cytoskeleton and CD34 fluorescence in a longitudinal section of a mouse kidney cortex. (a) F-Actin fluorescence. Inset: The green line marks the location of the kidney section. (b) CD34 immunofluorescence (red) (c) Merged image of (a) and (b). These images were generated by stitching together 1392 images taken in tile-scan mode. In the cortex, CD34 immunofluorescence is most intense in glomeruli, reflecting the complex capillary network within glomeruli. In the merged image (c), composed of F-Actin fluorescence and CD34 immunofluorescence, the glomeruli are seen in a yellowish-orange color because of the overlapping of the green (F-Actin) and red (CD34) fluorescence colors.

(Kumaran & Hanukoglu, 2020). Most of the tubules that appear in the peripheral cortex are proximal tubules with intense apical fluorescence reflecting the brush-border membranes (Figure 4).

The most striking observation of the CD34 immunofluorescence was that all the diverse types of tubules in the cortex are surrounded by capillaries (Figure 4). CD34 fluorescence encircles nearly every tubule except for contact sites between tubules (Figure 4). The

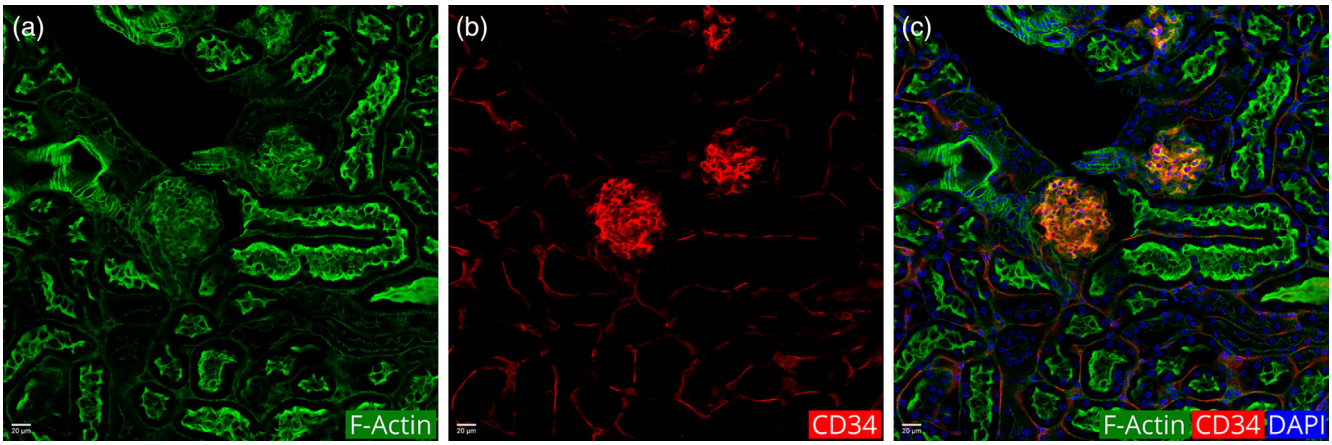

FIGURE 3 Close-up view of a Bowman's capsule and the proximal tubule segment extending from it. (a) Actin filaments. (b) CD34 immunofluorescence marking the capillary network. (c) Merged image of (a) and (b) with DAPI fluorescence of nuclei. The glomeruli in (B) show intense fluorescence due to the complex capillary network within the Bowman's capsule. The CD34 immunofluorescence also reveals the distribution of peritubular capillaries around renal tubule segments.

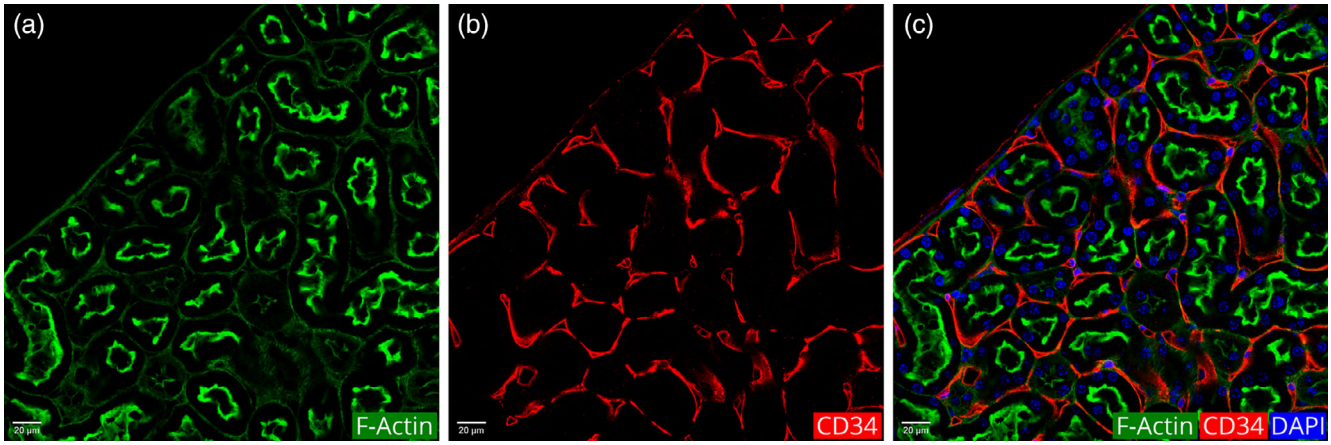

FIGURE 4 A magnified view of the cortical region showing the distribution of peritubular capillaries surrounding renal tubule segments. (a) F-Actin fluorescence (green). (b) CD34 immunofluorescence (red). (c) Merged image of (a) and (b) along with DAPI fluorescence of nuclei. The renal tubule segments, proximal tubules, distal tubules, and collecting ducts in the cortex could be identified by the criteria we established (Kriz & Kaissling, 2008). The CD34 fluorescence shows that the peritubular capillaries surround all of these different types of tubule segments.

peritubular capillaries form arcs around the basal surface of the renal tubule segments. Each tubule is wrapped by several arcs that cover most of the circumference of each tubule (Figure 4).

It is noteworthy that the red-colored CD34 fluorescence remains red even in the merged image (Figure 4), indicating that there does not appear to be a significant co-localization of F-actin and CD34 in the peritubular capillaries.

3.2 | Medullary regions

Similar to our analysis of the cortical region, we generated tile-scan images of cross-sections taken at a plane above the hilum (Figure 5a inset). This section was chosen to visualize both the cortical and outer medullary regions in one section. In contrast to the cortical section (Figure 1), this cross-section shows different shapes and intensities for both F-actin and CD34 (Figure 5). In the schematic diagram (Figure 5d), we marked the outlines of three concentric regions: (1) The outermost region that is the cortex; (2) the middle region that is the outer-stripe of the outer-medulla; and (3) the innermost region that is the inner-stripe of the outer-medulla.

The outermost cortical region presents an organization and composition similar to the cortical section in Figure 2.

3.3 | The border between the cortex and medulla

A characteristic feature at the border between the cortex and the medulla is the presence of blood vessels easily distinguished by their relatively large circular or oval cross-sections. These vessels show prominent thick and intense F-actin (green) and CD34 (red) fluorescence (Figure 5).

Figure 6 shows a magnified two-dimensional image of a single vessel (Figure 6a–c), and a three-dimensional reconstruction of

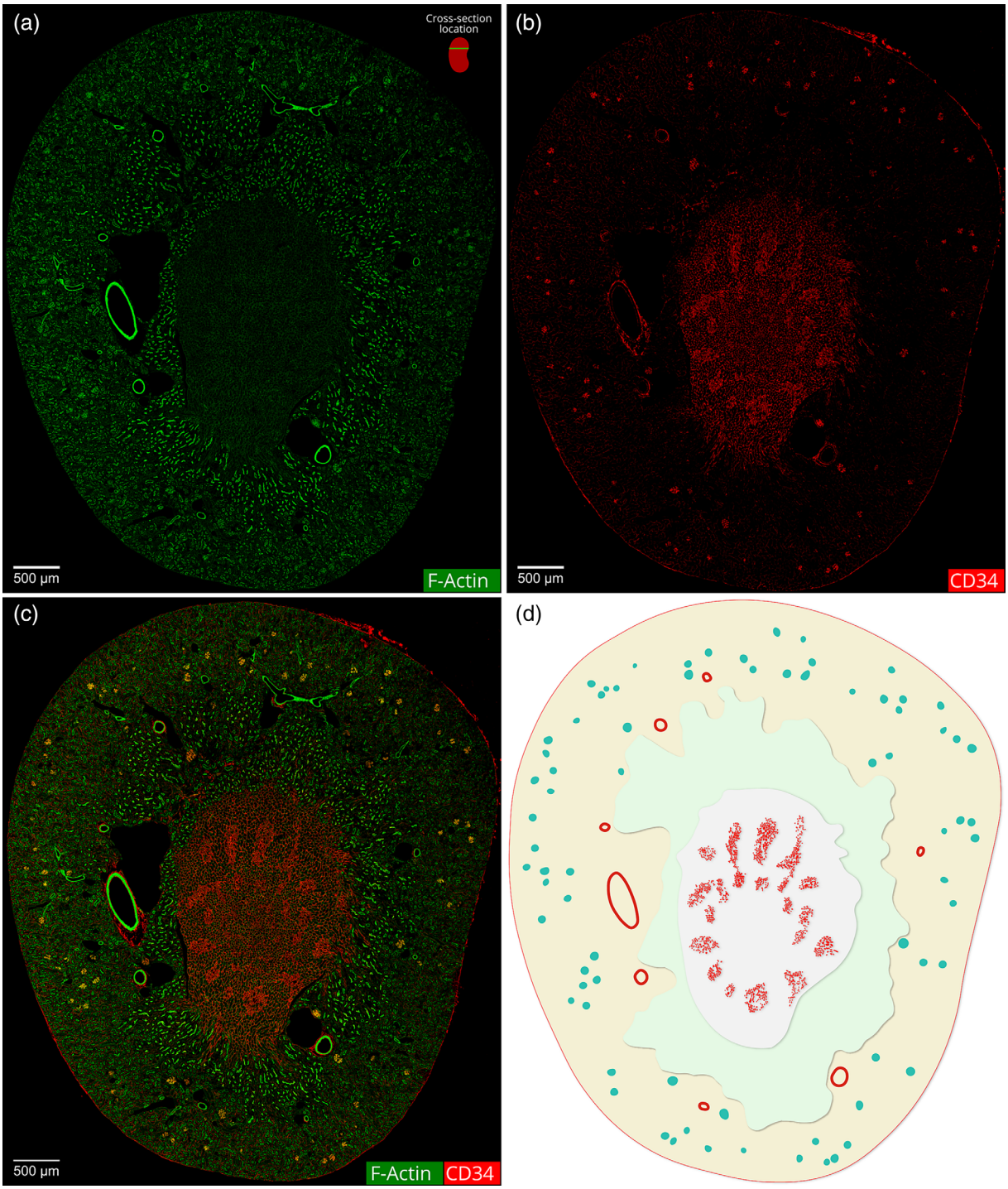

FIGURE 5 Actin cytoskeleton and CD34 fluorescence in a cross-section of a mouse kidney. This tile-scan image was produced by stitching together 1600 images in tile-scan mode. (a) Actin fluorescence (green). Inset: The green line marks the location of the kidney section above the hilum. (b) CD34 immunofluorescence (red) (c) Merged image of (a) and (b). (d) Schematic diagram of the section showing three regions that could be identified by the Actin cytoskeleton patterns and blood capillaries. These three regions, the cortex (C), the outer-stripe of the outer-medulla (OS), and the inner-stripe of the outer-medulla (IS), are marked by different background colors in the diagram. The most salient feature in the cortex is the glomeruli. In the central region of (b) and (c), CD34 immunofluorescence clearly marks clusters of capillaries.

the z-stack images from a 30 µm cross-section of a blood vessel (Figure 6d–f). In the 2D-image it can be seen that the blood vessel has a thin endothelial lining on the apical side showing specific CD34 immunofluorescence (Figure 6c). The nuclei of these endothelial cells are stained with DAPI. This thin endothelial lining is covered with a thick smooth muscle lining that shows intense F-actin fluorescence.

As previously shown (Treuting et al., 2018), in kidney cross-sections there are large vacuoles. These appear mostly in proximity to blood vessels (Figure 5).

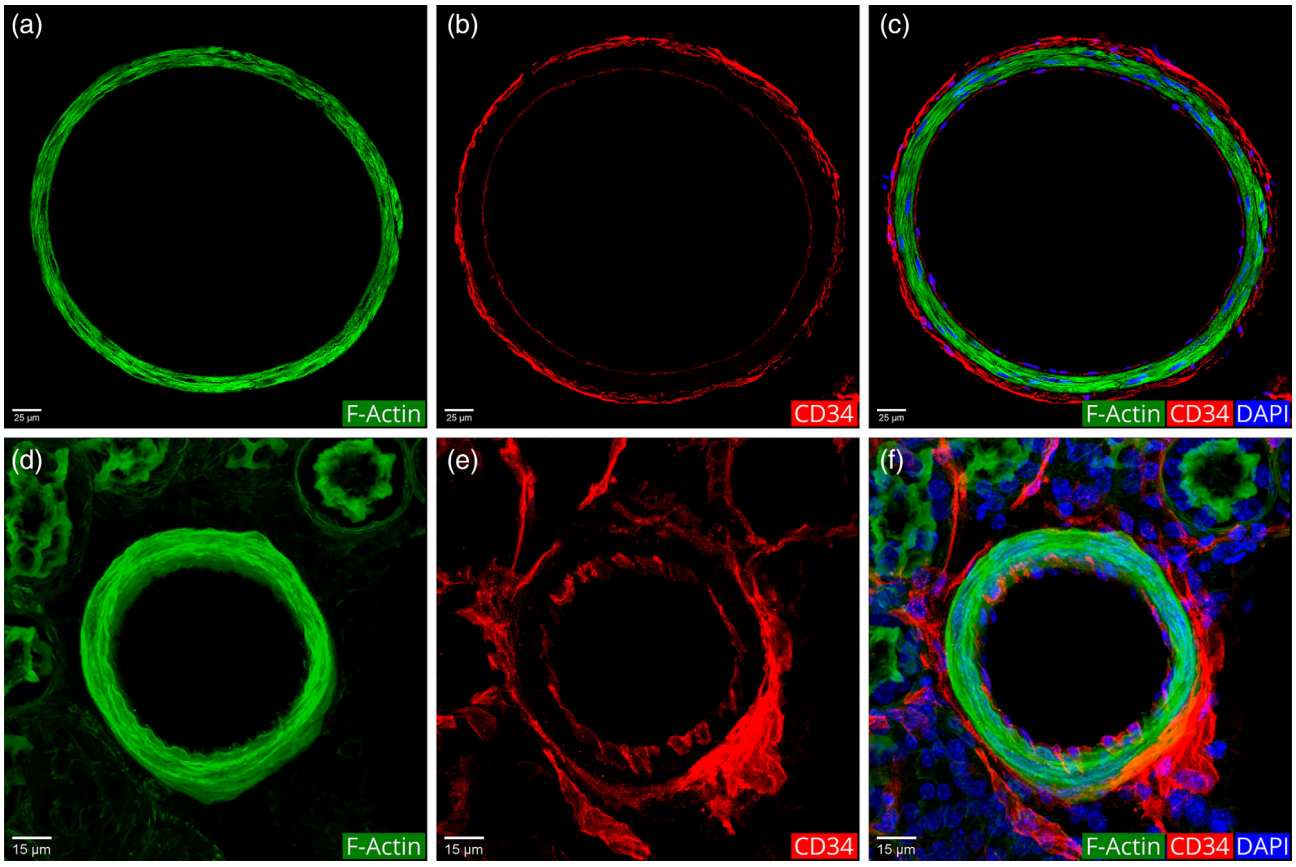

FIGURE 6 Expression of CD34 on the endothelial linings of a blood vessel from the cortex-medulla border region. (a) Actin fluorescence of the smooth muscle lining of the blood vessel. (b) CD34 immunofluorescence of the blood vessel. (c) Merged image of (a) and (b), including nuclear fluorescence of DAPI. (d–f) 3D z-stack image from 53 serial optical sections from the cortex-medulla border region. (d) Actin fluorescence. (e) CD34 immunofluorescence. (f) Merged images of (d) and (e) with nuclear fluorescence of DAPI.

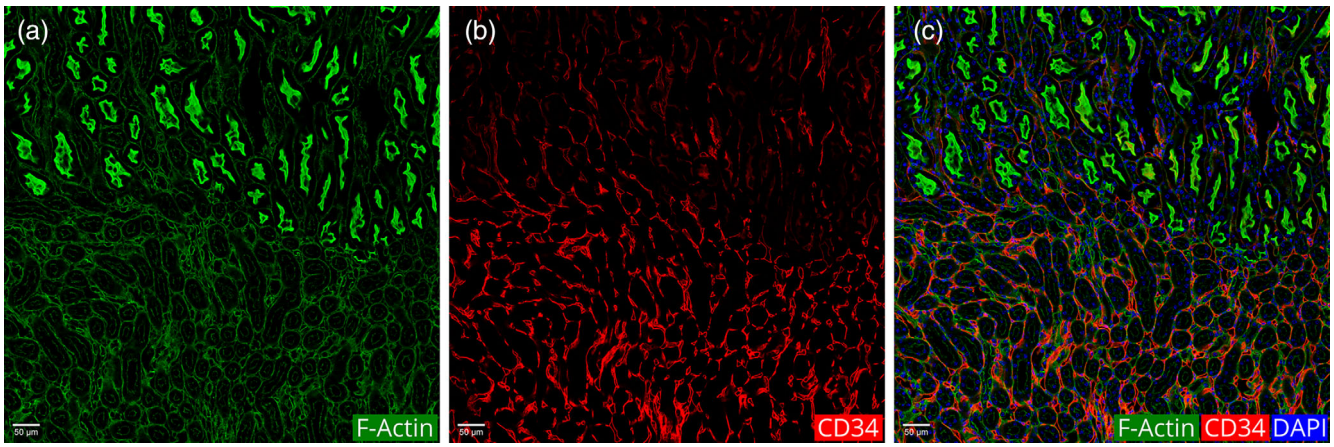

FIGURE 7 Magnified view of the transition zone between the outer and inner stripes of the outer medulla. (a) F-Actin fluorescence. (b) CD34 immunofluorescence. (c) Merged image of (a) and (b) with DAPI fluorescence of nuclei.

3.4 | The outer-stripe of the outer-medulla

The outer-stripe region of the outer-medulla differs from the cortex by the shapes and stronger intensities of the actin cytoskeleton (Figure 5). Figure 7 shows a magnified image of the transition zone between the outer-stripe and the inner-stripe of the outer medulla. As described previously, the transition zone between these regions is clearly distinguishable by the actin cytoskeletal patterns (Kumaran & Hanukoglu, 2020). The proximal tubule segments cease to appear at the border between the outer and inner stripes of the outer medulla (Figure 7).

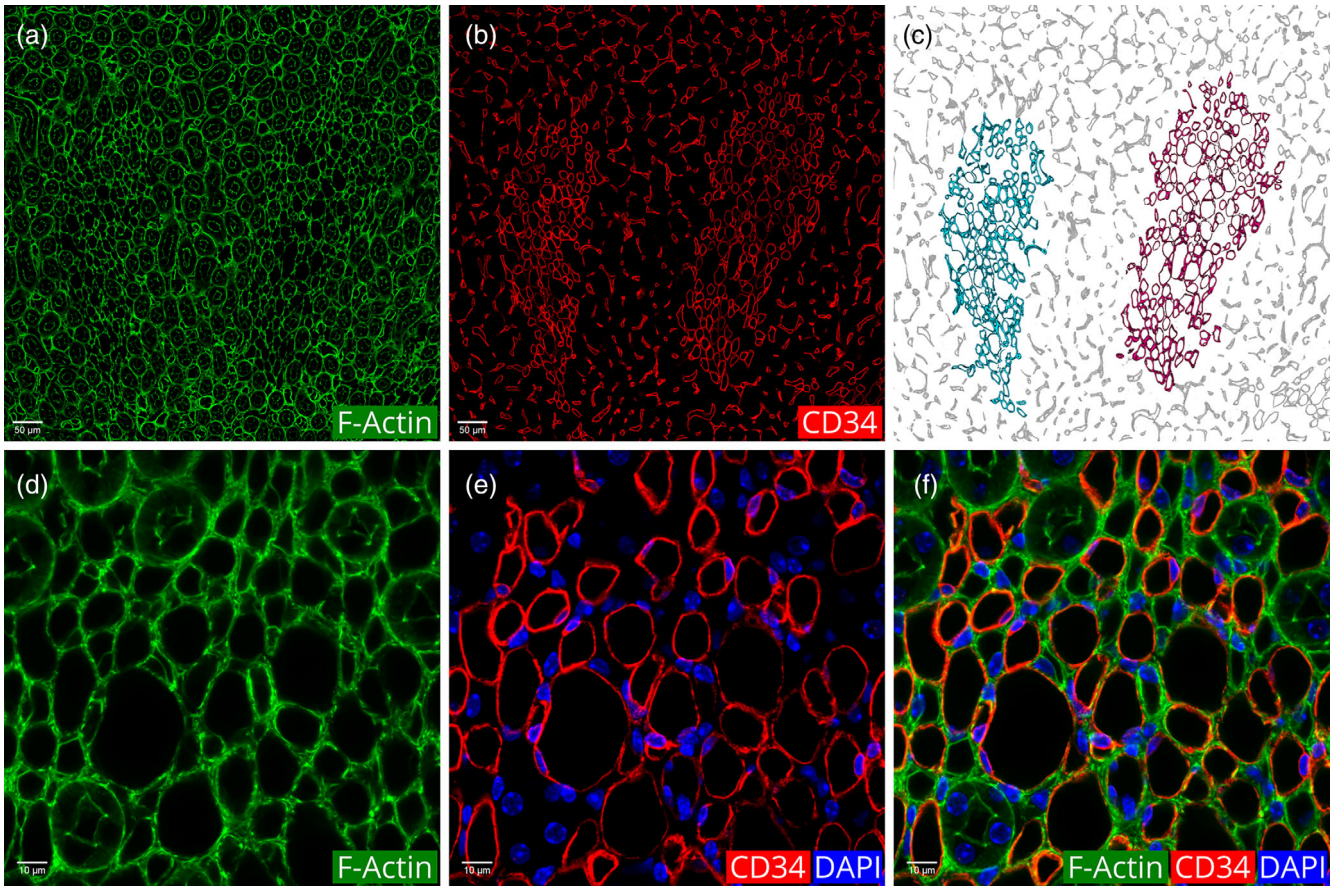

FIGURE 8 Vascular bundles in the outer medullary region of a mouse kidney. (a) Actin cytoskeleton patterns in the region of the vascular bundles. (b) CD34 immunofluorescence. (c) Schematic image of the vascular bundles based on (b). (d) Magnified image of the Actin filament patterns of vascular bundles. (e) CD34 immunofluorescence in the region along with nuclear fluorescence of DAPI. (f) Merged image of (d) and (e). Note that in the region of the vascular bundles, the CD34 immunofluorescence appears as a full circle. In contrast, in the arterioles attached to tubule segments, CD34 fluorescence appears in partial arcs around the tubule (Figure 3).

3.5 | The inner-stripe of the outer-medulla

The inner-stripe is delineated clearly by the high intensity of CD34 immunofluorescence and uniformly low intensity of F-actin fluorescence (Figure 5a,b).

In the inner-stripe region, CD34 immunofluorescence appears in intensely fluorescent clusters (Figure 5b). The diagram in Figure 5d shows these clusters. This diagram was produced by tracing the clusters in Figure 5d. As defined by the standard nomenclature for structures of the kidney (Kriz & Bankir, 1988), the clusters are vascular bundles, and the areas surrounding the clusters are the interbundle region.

3.6 | Vascular bundles in the inner-stripe

The vascular bundles (Figure 5d) are composed of thin vessels called descending and ascending vasa recta that return blood to arcuate veins (Ren et al., 2014). Figure 8 shows magnified images of these vascular bundles at two levels: (1) At the level of two individual clusters (Figure 8a–c). (2) At the level of blood vessels at a five-fold higher magnification (Figure 8d–f).

The most distinguishing aspect of the CD34 immunofluorescence in the vascular bundles is that the fluorescence appears as a complete circle reflecting the full cross-section of straight vessels (in Latin, vasa recta means "straight vessels") (Figure 8b,e). In contrast, in the arterioles attached to tubule segments, CD34 fluorescence appears in partial arcs around the tubule, reflecting the intertwined winding of the capillaries around the tubules (Figures 3 and 8b).

A second difference between the vasa recta and the peritubular capillaries is that the round cross-sections of the vasa recta also show a thin actin cytoskeleton on the circumference of the tubules (Figure 8d–f). In contrast, the peritubular capillaries do not show similar F-actin lined borders (Figure 3).

Within the clusters of vascular bundles there are easily visible tubule segments with thin walls of actin cytoskeleton but no CD34 fluorescence (Figure 8f). The second type of tubule is formed by thicker cells, again without any CD34 fluorescence (Figure 8f). According to the key we established, these are respectively thin limbs of Henle's loop and thick ascending limbs (Kumaran & Hanukoglu, 2020).

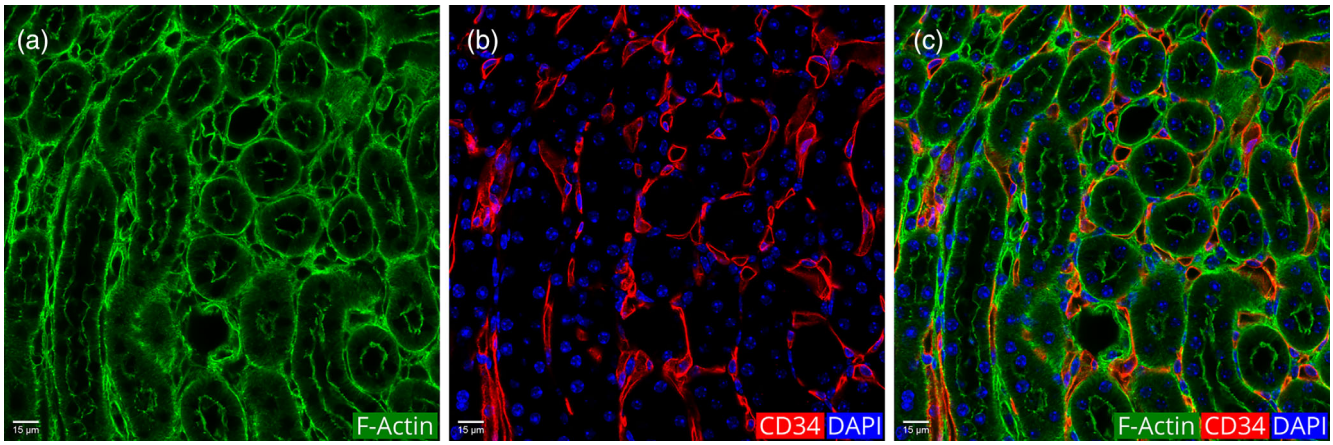

FIGURE 9 Magnified view of the interbundle region of the inner-stripe. (a) F-Actin fluorescence. (b) CD34 immunofluorescence. (c) Merged image of (a) and (b) with DAPI fluorescence of nuclei. In this image, two types of nephron segments are visible: Thick ascending limbs, and collecting ducts. CD34 immunofluorescence is observed in the peritubular capillaries intertwined with the tubules.

Notably, the tubules among the vasa recta do not have intertwined peritubular capillaries. In both low and high magnification of CD34 immunofluorescence, partial arcs are seen only in the interbundle region between bundles. Similar arcs do not appear within the vascular bundles (Figure 8b,e).

Ren et al. generated a 3-dimensional reconstruction of vascular bundles in mouse kidney (Ren et al., 2014). Our identifications are consistent with their diagrammatic representation of the vascular bundle components (Figure 9 in the Ren et al. paper).

3.7 | Interbundle region in the inner-stripe

The interbundle region between the vascular bundles contains descending thin limbs of the loops of Henle, thick ascending limbs of the loops of Henle, and collecting ducts (Pannabecker, 2013; Ren et al., 2014). In our mapping of the renal actin cytoskeleton, we identified the key features of these tubule segments (Kumaran & Hanukoglu, 2020). Figure 9 shows a magnified view of the interbundle region with thick ascending limbs and collecting ducts. Similar to the picture observed in the cortex (Figure 4), the tubules are surrounded by arcs of CD34 immunofluorescence that mark the peritubular capillaries intertwined with the tubules (Figure 9).

3.8 | Inner medulla

In the mouse kidney, the largest area of the inner medulla appears at medially located cross-sections close to the hilum. Therefore, to examine the structure of the mouse kidney inner medulla, we took sections at a plane close to the hilum. In such a cross-section, CD34 immunofluorescence appears as irregular circles or polygons (Figure 10). These represent cross-sections of descending vasa recta and ascending vasa recta that join the vascular bundles in the inner-stripe (Kriz & Kaissling, 2008).

According to the criteria we established (Kumaran & Hanukoglu, 2020), F-actin fluorescence in the inner medulla reveals two types of tubule segments: thin limbs of the loop of Henle and collecting ducts (Figure 10). Similar to the vascular bundle region (Figure 8), no arcs of CD34 immunofluorescence are seen around these tubules, that is, tubule segments in the inner medulla are not surrounded by peritubular capillaries. CD34 fluorescence marking the capillaries appears as a full circle or a polygon located between the tubules (Figure 10).

3.9 | Papilla

At its broadest part, the inner medulla tapers, forming a crest called papilla. This region contains the most distal portions of the collecting ducts that merge to form large ducts called papillary ducts, which are also known as the ducts of Bellini (Pannabecker, 2013). The urine in the papillary ducts empties into the renal calyx and from there flows into the ureter.

The cells that form the papillary ducts are more cuboidal in shape and have thicker lateral F-actin bundles between cell borders (Figure 11). CD34 immunofluorescence marks capillaries alongside the ducts (Figure 11). The vessels appear to be straight and not intertwined with the tubules, as seen in the cortex (Figure 3) and outer (Figure 4) and inner stripes (Figure 8) of the outer medulla.

4 | DISCUSSION

In this study, for the first time, we produced high-resolution images of renal tubule segments and peritubular capillaries in entire sections of a kidney wherein the cellular borders of the epithelia and the borders of the peritubular capillaries are clearly visualized. We call these images "cytoskeletal maps." Our cytoskeletal maps delineate the

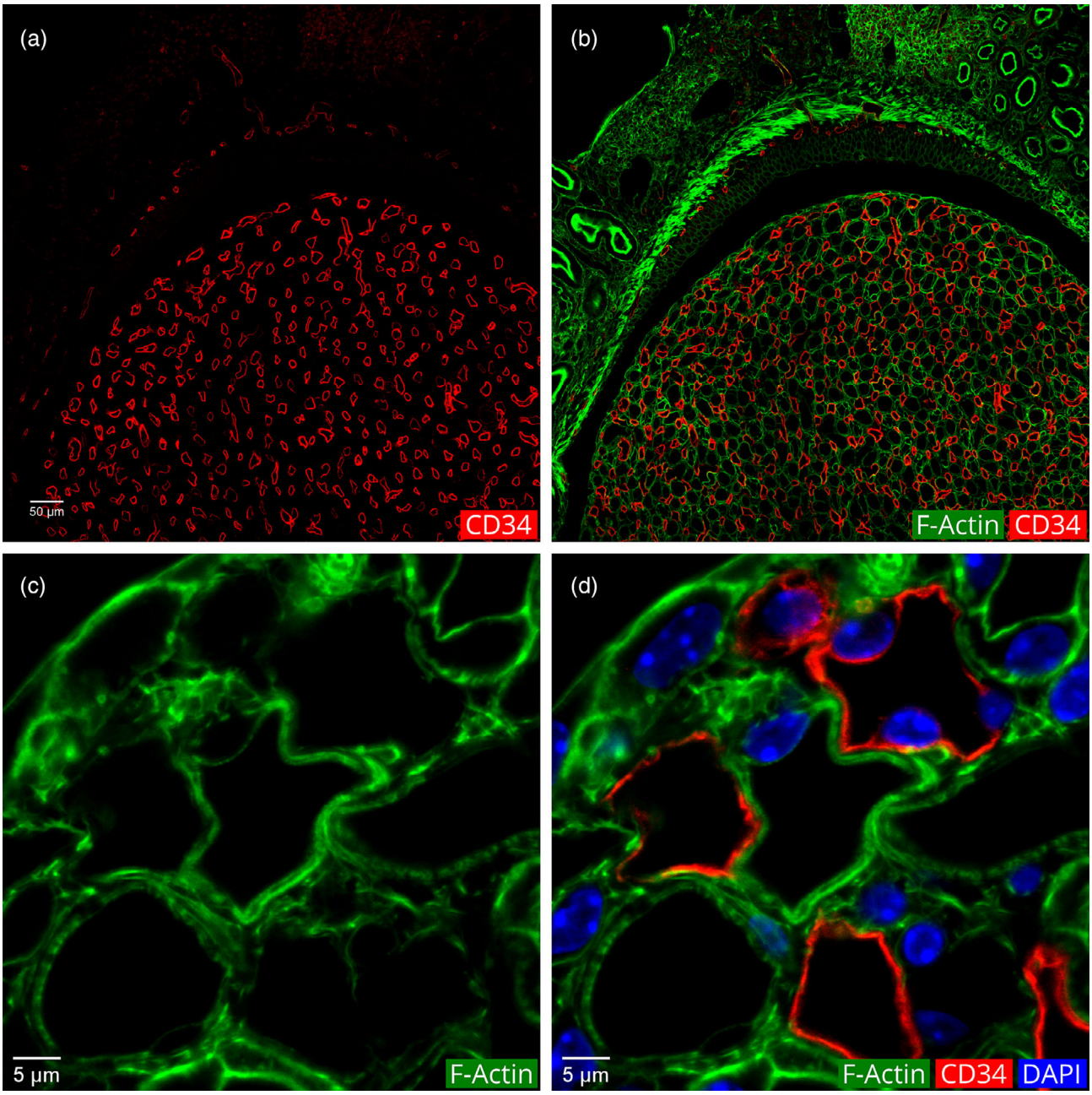

FIGURE 10 Distribution of capillaries in the inner medullary region. The capillaries appear between the renal tubule segments and have mostly circular outlines. (a) CD34 immunofluorescence in the inner medullary region. (b) Merged image of (a) with F-Actin fluorescence. (c) Magnified image of an inner medullary region showing thin loops and collecting ducts. (d) Merged image of (C) with CD34 immunofluorescence.

major regions of the kidney, including the cortex, the outer and inner stripes of the outer medulla, the inner medulla, and the papilla without any histological staining (Figure 5).

The cytoskeletal maps we generated with two markers are consistent with previous studies that used multiple biomarkers and complex methods, such as silicone rubber (microfil) injection into renal vasculature (Fan et al., 2019; Kriz & Kaissling, 2008). Besides providing a whole tissue section image, the present method allows the visualization of cellular architecture and cellular borders.

About 95% of the volume of the kidney is occupied by the repeating structural units of renal tubules, the network of capillaries intertwined with these tubules, and additional blood vessels. Thus, the method employed here allows visualization of the structural organization of ~95% of the total kidney volume. The remaining interstitial space between the renal tubules is filled mainly by fibroblasts responsible for the production of the extracellular matrix, and dendritic cells (Kriz & Kaissling, 2008; Lamley & Kriz, 1991; Zeisberg & Kalluri, 2015). These cells are not distinguished in our maps.

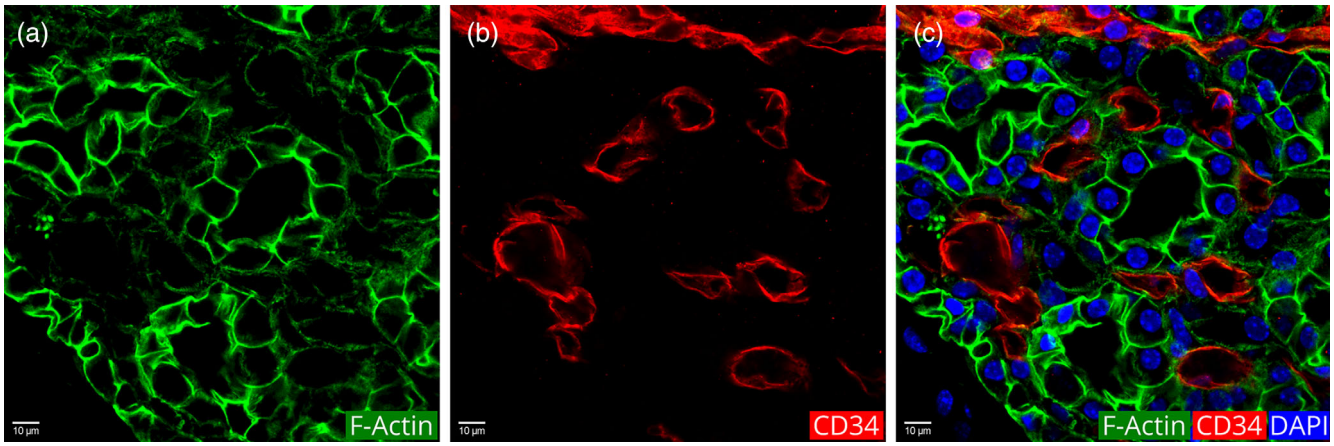

FIGURE 11 Distribution of blood capillaries in the papillary region. The papillary ducts are not surrounded by peritubular capillaries. Capillaries appear in the spaces between papillary ducts. (a) Actin filament fluorescence of the papillary region. (b) CD34 immunofluorescence. (c) Merged images of (a) and (b) with nuclear fluorescence of DAPI.

In all kidney regions, both the basement membrane and the luminal membrane show varying intensities of F-actin fluorescence, the strongest being in the brush-border membrane of the proximal tubules. However, F-actin bundles on the lateral borders between cells are visualized only in the collecting ducts (Figure 10). The most intense F-actin fluorescence on the lateral borders is observed in the epithelial cells of the renal papilla (Figure 11). It has been suggested that a dense cytoskeleton may have developed to withstand the osmotic pressure in the collecting ducts (Kriz & Kaissling, 2008).

AUTHOR CONTRIBUTIONS

Girishkumar Kaitholil Kumaran and Israel Hanukoglu conceived and designed the research together. Girishkumar Kaitholil Kumaran performed the experiments and prepared the samples for microscopy. Both authors worked together on image collection, analysis and generation of figures. Girishkumar Kaitholil Kumaran and Israel Hanukoglu drafted the manuscript jointly.

ACKNOWLEDGMENTS

This research was partially supported by funds from Ariel University.

CONFLICT OF INTEREST STATEMENT

The authors declare no conflict of interest.

ORCID

Girishkumar Kaitholil Kumaran https://orcid.org/0000-0003-3000-7978

Israel Hanukoglu https://orcid.org/0000-0003-3889-0320

REFERENCES

Al-Katib, S., Shetty, M., Jafri, S. M. A., & Jafri, S. Z. H. (2017). Radiologic assessment of native renal vasculature: A multimodality review. *Radiographics*, *37*, 136–156. https://doi.org/10.1148/rg.2017160060

Cullen-McEwen, L., Sutherland, M. R., & Black, M. J. (2016). The human kidney: Parallels in structure, spatial development, and timing of nephrogenesis. In M. H. Little (Ed.), *Kidney development, disease, repair and regeneration* (pp. 27–40). Academic Press. https://doi.org/10.1016/B978-0-12-800102-8.00003-5

Fan, L., Wang, S., He, X., Gonzalez-Fernandez, E., Lechene, C., Fan, F., & Roman, R. J. (2019). Visualization of the intrarenal distribution of capillary blood flow. *Physiological Reports*, *7*, e14065. https://doi.org/10.14814/phy2.14065

Hassanpour, M., Salybekov, A. A., Kobayashi, S., & Asahara, T. (2023). CD34 positive cells as endothelial progenitor cells in biology and medicine. *Frontiers in Cell and Development Biology*, *11*, 1128134. https://doi.org/10.3389/FCELL.2023.1128134

Kriz, W., & Bankir, L. (1988). A standard nomenclature for structures of the kidney. The Renal Commission of the International Union of Physiological Sciences (IUPS). *Kidney International*, *33*, 1–7. https://doi.org/10.1152/ajprenal.1988.254.1.F1

Kriz, W., & Kaissling, B. (2008). Structural organization of the mammalian kidney. *Seldin and Giebisch's the Kidney*, *1*, 479–563. https://doi.org/10.1016/B978-012088488-9.50023-1

Kumaran, G. K., & Hanukoglu, I. (2020). Identification and classification of epithelial cells in nephron segments by actin cytoskeleton patterns. *The FEBS Journal*, *287*, 1176–1194. https://doi.org/10.1111/febs.15088

Lamley, K. V., & Kriz, W. (1991). Anatomy of the renal interstitium. *Kidney International*, *39*, 370–381. https://doi.org/10.1038/ki.1991.49

Nordsletten, D. A., Blackett, S., Bentley, M. D., Ritman, E. L., & Smith, N. P. (2006). Structural morphology of renal vasculature. *American Journal of Physiology. Heart and Circulatory Physiology*, *291*, H296–H309. https://doi.org/10.1152/ajpheart.00814.2005

Pannabecker, T. L. (2013). Comparative physiology and architecture associated with the mammalian urine concentrating mechanism: Role of inner medullary water and urea transport pathways in the rodent medulla. *American Journal of Physiology – Regulatory Integrative and Comparative Physiology*, *304*, R488–R503. https://doi.org/10.1152/ajpregu.00456.2012

Pusztaszeri, M. P., Seelentag, W., & Bosman, F. T. (2006). Immunohistochemical expression of endothelial markers CD31, CD34, von Willebrand factor, and Fli-1 in normal human tissues. *The Journal of Histochemistry and Cytochemistry*, *54*, 385–395. https://doi.org/10.1369/jhc.4A6514.2005

Ren, H., Gu, L., Andreasen, A., Thomsen, J. S., Cao, L., Christensen, E. I., & Zhai, X.-Y. (2014). Spatial organization of the vascular bundle and the interbundle region: Three-dimensional reconstruction at the inner stripe of the outer medulla in the mouse kidney. *American Journal of Physiology. Renal Physiology*, *306*, F321–F326. https://doi.org/10.1152/ajprenal.00429.2013

Rodrigues, C. R., Moga, S., Singh, B., & Aulakh, G. K. (2023). CD34 protein: Its expression and function in inflammation. *Cell and Tissue Research*, *393*, 443–454. https://doi.org/10.1007/s00441-023-03811-4

Sequeira Lopez, M. L. S. (2016). The origin and regulation of the renal vasculature. In M. H. Little (Ed.), *Kidney development, disease, repair and regeneration* (pp. 147–162). Elsevier. https://doi.org/10.1016/b978-0-12-800102-8.00013-8

Sharma, S., Kumaran, G. K., & Hanukoglu, I. (2020). High-resolution imaging of the actin cytoskeleton and epithelial sodium channel, CFTR, and aquaporin-9 localization in the vas deferens. *Molecular Reproduction and Development*, *87*, 305–319. https://doi.org/10.1002/mrd.23317

Treuting, P. M., Dintzis, S. M., & Montine, K. S. (2018). *Comparative anatomy and histology: A mouse, rat and human atlas* (2nd ed.). Academic Press.

Zeisberg, M., & Kalluri, R. (2015). Physiology of the renal interstitium. *Clinical Journal of the American Society of Nephrology*, *10*, 1831–1840. https://doi.org/10.2215/CJN.00640114

How to cite this article: Kumaran, G. K., & Hanukoglu, I. (2023). Mapping the cytoskeletal architecture of renal tubules and surrounding peritubular capillaries in the kidney. *Cytoskeleton*, 1–11. https://doi.org/10.1002/cm.21809